Group 4 Transition-Metal Atom Reactions with CS_2 and OCS: Infrared Spectra and Density Functional Calculations of SMCS, SM-(η^2-CS), SMCO, and OMCS in Solid Argon

Alexander B. Baker and Lester Andrews*

Department of Chemistry, University of Virginia, P.O. Box 400319 Charlottesville, Virginia 22904-4319

Received: July 13, 2006; In Final Form: September 14, 2006

Laser-ablated titanium, zirconium, and hafnium atoms were reacted with CS_2 and OCS molecules during condensation in excess argon. With CS_2, the SMCS and S−M(η^2-CS) products were formed on sample deposition. Photolysis increased both complexes, while annealing favored the lower energy S−M(η^2-CS) side-bound isomer. The OCS reactions produced SMCO, OMCS, and the simple M(η^2-CO)S adduct. Product absorptions are identified by comparison with density functional theory frequency calculations and isotopic substitutions. Investigations with OCS emphasized differences in the CS and CO bond insertion products.

Introduction

Structural isomerism is an important part of chemistry, which includes the issue of end-bound and side-bound ligands.[1] Crystallographic evidence for photoreversible side-on coordination of N_2 to a single osmium metal ion center has been communicated.[2] We have recently reported in this journal that group 3 transition-metal SMCS and SM(η^2-CS) isomers are interconverted on sample irradiation and annealing.[3] Density functional calculations found that the side-bound isomer is slightly higher in energy than the end-bound isomer. We wish to report here the analogous group 4 end-bound and side-bound isomers and rearrangement on sample annealing where the side-bound isomer is now lower in energy on the basis of DFT calculations. In contrast, previous work with Ti and CO_2 complexes found the side-bound isomer to be less stable,[4] and late transition-metal CS_2 reactions formed only the insertion SMCS isomer without the side-bound analogue.[5]

Experimental and Computational Methods

The experimental methods for laser ablation and matrix isolation to characterize new metal atom reaction products have been described and referenced in our recent group 3 article.[3] Low ablation energy was employed to minimize the contribution of metal cluster species. Similar DFT calculations were also performed for group 4 complexes to support the experimental work. The B3LYP and BPW91 density functionals in the Gaussian 98 program system were used with the basis sets 6-311+(2d) for nonmetals and an SDD pseudopotential for metals in all calculations.[6−13] These functionals and basis sets were selected to be compatible with those used for similar chemical systems[3−5] because a modest basis set calculation works well and can be run in a reasonable time for transition-metal sulfur species[3,5] and other transition-metal compounds.[14] Geometries were fully optimized and frequencies were computed analytically, and reported energies include zero-point but not temperature corrections. Reaction product total electronic energies were calculated to show that the products are more stable than reactant atom and precursor molecule. Product isotopic frequencies were computed (not scaled and not corrected for anharmonicity) to provide a guide for assigning the experimental spectra.

Results

Infrared Spectra. Infrared spectra are reported for laser-ablated titanium, zirconium, and hafnium co-deposited with CS_2 in argon. Product absorptions are shown in Tables 1−3, and representative spectra are shown in Figures 1−3, including photolysis and annealing behavior. In each figure, previously reported diatomic CS absorptions[15] are marked for comparison when appropriate, and absorptions for the very stable MO_2 molecules also appear from the favorable reaction with trace O_2 impurity.[16] Isotopes $^{13}C^{32}S_2$ and $^{12}C^{34}S_2$ were also employed to facilitate vibrational mode assignments. Analogous experiments were also performed for reactions of group 4 transition metals with OCS in argon. Because of impurities in the OCS sample, CO_2 reaction products were also observed.[3,4] Product absorptions are reported in Table 4, and Figure 4 contains representative spectra for each of the transition metals.

Calculations. Relaxed geometries, stable energies, and vibrational frequencies were calculated for the MCS_2 isomers SMCS and SM(η^2-CS). The results are summarized in Tables 1−3 and in Figure 5. The ^{1}A electronic state was lower in energy than the next triplet spin state by approximately 10 kcal/mol for SMCS and 30 kcal/mol for SM(η^2-CS). This information was then applied to the analogous OCS calculations, and the major products were computed (SMCO, OMCS, SM(η^2-CO), and OM(η^2-CS)), taking into account the possibility of CS or CO insertion. Spin multiplicities were again considered: for SMCO and OMCS, the singlet spin state was approximately 15 and 30 kcal/mol lower in energy than the triplet state, respectively.

As a calibration for the calculation of frequencies and bond lengths, the stable precursor molecules were computed for comparison with literature values.[17] The strong antisymmetric bond stretching fundamental of SCS was computed as 1531 cm^{-1} by B3LYP and 1518 cm^{-1} using BPW91 and bond lengths as 1.558 and 1.567 Å, respectively. The argon matrix SCS fundamental is observed at 1528 cm^{-1} and the bond length is 1.56 Å. Our calculations bracket experimental values and serve as a good prediction for these experimental quantities. A like

* Author to whom correspondence should be addressed. E-mail: lsa@virginia.edu.

10.1021/jp064433l CCC: $33.50
Published on Web 11/04/2006

TABLE 1: Observed Frequencies and Frequencies and Intensities Calculated at Different Levels of Theory for the S−Ti−C═S and S−Ti−(η^2-C═S) Products in the Ti + CS_2 Reaction[a]

(a) S−Ti−C═S

	S−Ti−C═S					^{34}S−Ti−C═^{34}S			S−Ti−^{13}C═S		
approx mode	obs	calc[b]	int	calc[c]	int	obs	calc[b]	int	obs	calc[b]	int
C═S stretch	1228.6/1223.9/ 1219.6/1212.9	1236.7	442	1203.2	276	1221.6/1217.0/ 1212.7/1208.1	1229.6	43 7	1190.8/1185.9/ 1181.7/1175.8	1198.1	414
Ti−S stretch	553.6	577.0	92	565.4	57	543.5	567.0	89	553.2	576.9	92
Ti−C stretch		449.2	5	453.2	10		444.1	5		446.0	4
S−C−Ti bend		264.3	1	267.7	1		262.7	1		256.5	1
S−C−Ti bend o.p.		221.1	50	213.6	48		220.5	51		213.6	47
S−Ti−C═S distort		84.1	8	85.0	7		82.1	8		83.9	8

(b) S−Ti−(η^2-C═S)

	S−Ti−(η^2-C−S)					^{34}S−Ti−(η^2-C−^{34}S)			S−Ti−(η^2-^{13}C−S)		
approx mode	obs	calc[b]	int	calc[c]	int	obs	calc[b]	int	obs	calc[b]	int
C−S stretch	963.0/956.8/952.4	927.7	85	894.8	59	954.9/948.7/944.5	919.6	83	936.7/931.1/926.9	902.5	81
Ti−C stretch		593.1	23	600.2	22		592.6	24		579.2	55
Ti−S stretch		578.1	79	556.2	52		568.3	75		574.6	46
S−C−Ti bend		347.2	3	349.6	4		341.7	3		345.5	3
S−Ti−C bend		184.5	3	181.3	2		183.3	3		179.5	2
S−Ti−C═S distort		137.6	5	138.4	4		134.5	4		137.4	5

[a] Frequencies and intensities are in cm^{-1} and km/mol. Intensities are all calculated values. [b] B3LYP/6-311+G(2d)/SDD. [c] BPW91/6-311+G(2d)/SDD.

TABLE 2: Observed Frequencies and Frequencies and Intensities Calculated at Different Levels of Theory for the S−Zr−C═S and S−Zr−(η^2-C═S) Products in the Zr + CS_2 Reaction[a]

(a) S−Zr−C═S

	S−Zr−C═S					^{34}S−Zr−C═^{34}S			S−Zr−^{13}C═S		
approx mode	obs	calc[b]	int	calc[c]	int	obs	calc[b]	int	obs	calc[b]	int
C═S stretch	1202.5/1199.5/ 1196.2/1189.4	1212.8	398	1186.2	296	1195.9/1193.2/ 1189.7/1182.9	1206.0	393	1165.2/1162.2/ 1159.1/1152.4	1174.7	374
Zr−S stretch	502.5	516.1	72	507.6	50	492.5	505.0	69	502.5	516.0	72
Zr−C stretch		399.4	4	399.8	6		394.1	4		395.3	4
S−C−Zr bend		257.9	1	259.9	2		256.0	1		250.5	1
S−C−Zr bend o.p.		228.9	52	223.6	50		228.2	52		221.0	48
S−Zr−C═S distort		77.7	6	77.1	5		75.8	5		77.6	6

(b) S−Zr−(η^{2-}C═S)

	S−Zr−(η^2-C−S)					^{34}S−Zr−(η^2-C−^{34}S)			S−Zr−(η^2-^{13}C−S)		
approx mode	obs	calc[b]	int	calc[c]	int	obs	calc[b]	int	obs	calc[b]	int
C−S stretch	933.4/929.1	905.0	75	877.0	55	925.6/921.6	897.0	74	908.3/903.6	853.1	53
Zr−C stretch		560.0	29	559.5	25		559.4	30		541.8	23
Zr−S stretch		509.5	70	494.9	49		498.8	67		493.9	49
S−C−Zr bend		316.6	3	321.0	3		310.5	3		319.7	3
S−Zr−C bend		185.9	4	182.2	4		184.7	4		177.1	3
S−Zr−C═S distort		123.8	3	124.4	3		120.9	3		124.2	3

[a] Frequencies and intensities are in cm^{-1} and km/mol. Intensities are all calculated values. [b] B3LYP/6-311+G(2d)/SDD. [c] BPW91/6-311+G(2d)/SDD.

result is found for OCS. The B3LYP values are 2100 and 866 cm^{-1} and 1.156 and 1.568 Å and the BPW91 computations give 2048 and 854 cm^{-1} and 1.169 and 1.573 Å. The argon matrix OCS frequencies are 2047 and 854 cm^{-1} and the bond lengths are 1.16 and 1.56 Å. Typically, B3LYP frequencies are slightly higher than observed values and BPW91 computations are closer to the experimental values.[18]

For Ti, Zr, and Hf, the SMCS product was calculated to be the most stable, followed closely by the SM(η^2-CS) product. For the CS_2 reactions, the relative B3LYP product energies with respect to reactants for S−Ti−CS, S−Zr−CS, and S−Hf−CS were −29, −66, and −48 kcal/mol, respectively. With the BPW91 method, these were −60, −92, and −82 kcal/mol, respectively. Predicted B3LYP energies of S−Ti(η^2-CS), S−Zr-(η^2-CS), and S−Hf(η^2-CS) were −37, −71, and −62 kcal/mol, respectively. With BPW91, the relative energies were −67, −100, and −100 kcal/mol, respectively. Attempts to calculate a preinsertion adduct M(η^2-CS)S led directly to the stable insertion product SMCS. In addition, the B3LYP functional predicted that the simple M(η^2-S_2)C adduct would be more stable by 4 kcal/mol for Ti and Hf but less stable by 3 kcal/mol for Zr. The BPW91 method supports this finding. However, the calculated frequencies for M(η^2-S_2)C (with Ti, Zr, or Hf) are below our limit of detection. For this reason, only S−M−CS and S−M(η^2-CS) products are considered. Relative B3LYP electronic energies for these products as compared to atom and precursor molecule energies are given in Figure 5 along with their calculated geometries. We make no case for the absolute accuracy of these calculated product electronic energies since these are new molecules. However, these calculated energies show that the products are more stable than reactants, which is a necessary condition for the formation of new product

TABLE 3: Observed Frequencies and Frequencies and Intensities Calculated at Different Levels of Theory for the S−Hf−C═S and S−Hf−(η^2−C═S) Products in the Hf + CS_2 Reaction[a]

(a) S−Hf−C═S

	S−Hf−C═S					^{34}S−Hf−C═^{34}S			S−Hf−^{13}C═S		
approx mode	obs	calc[b]	int	calc[c]	int	obs	calc[b]	int	obs	calc[b]	int
C═S stretch	1216.4/1214.3/ 1210.0/1203.4	1223.6	33 1	1196.0	267	1210/1207.9/ 1203.9/1195.8	1217.1	326	1177.8/1175.6/ 1171.7/1165.2	1184.5	312
Hf−S stretch	489.9/484.9	485.7	55	476.9	39	477.9/473.1	474.1	52	489.9/484.4	486.0	55
Hf−C stretch		384.7	4	384.0	4		379.3	4		380.2	4
S−C−Hf bend		264.4	2	274.9	2		262.3	2		257.1	1
S−C−Hf bend o.p.		241.7	46	264.8	2		240.9	46		233.3	42
S−Hf−C ═S distort		78.7	5	76.4	4		76.7	5		78.7	5

(b) S−Hf−(η^2−C═S)

	S−Hf−(η^2-C−S)					^{34}S−Hf−(η^2-C−^{34}S)			S−Hf−(η^2-^{13}C−S)		
approx mode	obs	calc[b]	int	calc[c]	int	obs	calc[b]	int	obs	calc[b]	int
C−S stretch	875.1	848.3	67	825.0	49	867.6	840.4	66	852.9	825.8	64
Hf−C stretch		561.5	35	558.8	24		561.2	35		541.5	31
Hf−S stretch		478.7	53	466.8	37		466.9	50		478.5	54
S−C−Hf bend		310.4	2	311.7	2		303.5	2		309.1	2
S−Hf−C bend		188.0	5	186.7	5		186.7	5		182.6	4
S−Hf−C ═S distort		120.0	3	121.7	2		117.0	3		119.8	3

[a] Frequencies and intensities are in cm^{-1} and km/mol. Intensities are all calculated values. [b] B3LYP/6-311+G(2d)/SDD. [c] BPW91/6-311+G(2d)/SDD.

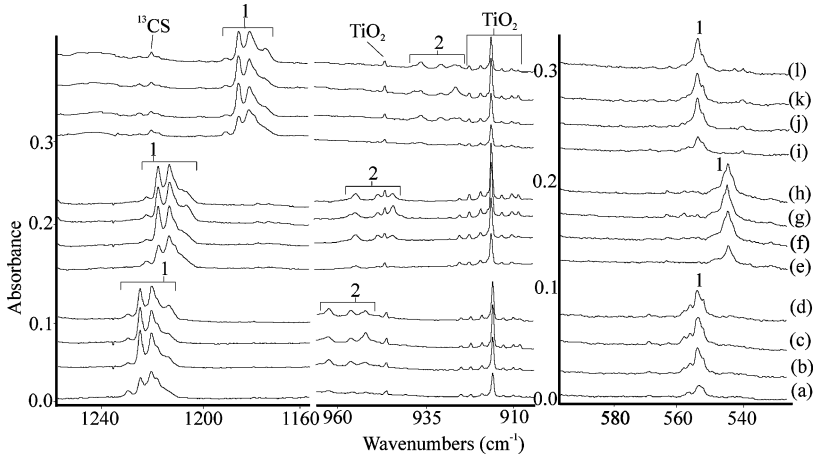

Figure 1. Infrared spectra in the 1260−1160, 960−910, and 600−520 cm^{-1} regions for Ti and CS_2. (a) After 30-min ablation of Ti with 0.5% $^{12}C^{32}S_2$ co-deposited in argon at 8 K, (b) after 10 min of mercury arc lamp irradiation $\lambda > 290$ nm, (c) after annealing to 25 K, and (d) after 10 min broad-band ($\lambda > 220$ nm) irradiation. (e) Deposition of Ti + $^{12}C^{34}S_2$, (f) $\lambda > 290$ nm irradiation, (g) annealing to 25 K, and (h) broad-band irradiation. (i) Deposition of Ti + $^{13}C^{32}S_2$, (j) $\lambda > 290$ nm irradiation, (k) annealing to 25 K, and (l) broad-band irradiation. Labels 1 and 2 refer to the STiCS and STi(η^2-CS) products, respectively.

molecules. Furthermore, by differences within a pair of calculations for structural isomers, the ring isomer is more stable that the open form by 5−15 kcal/mol. Hence, energy differences are expected to be meaningful. Both hybrid and pure density functionals have been used to calculate transition-metal MCO electron affinities, and these can be compared with experimental observations. In a series of first-row transition-metal monocarbonyls, both functionals predicted the electron affinities within 20%.[14b] Several first-row oxide and fluoride binding energies were recently computed within 10% of the experimental values using the B3LYP functional and a modest basis set.[14c] Hence, we believe that the B3LYP energies presented here clearly show that these product molecules are more stable than the reactants and that the cyclic isomers are probably more stable than the open SMCS structures.

In principle, the OCS reaction could yield CS and CO insertion, and calculations were performed for both. Ultimately, CS insertion was favored, resulting in singlet spin state SMCO and SM(η^2-CO) complexes. The SMCO product for Ti, Zr, and Hf was found to be −37, −67, and −53 kcal/mol more stable than reactants, respectively, using the B3LYP method. The SM(η^2-CO) adduct was less stable with B3LYP energies of −30, −58, and −46 kcal/mol, respectively. Taking CO insertion into account instead, OMCS energies with B3LYP were −22, −48, and −35 kcal/mol for Ti, Zr, and Hf, respectively. Interestingly, the OM(η^2-CS) isomer was more stable, almost to the extent of its CS insertion counterpart, SM(η^2-CO), with B3LYP energies of −29, −57, and −46 kcal/mol for Ti, Zr, and Hf, respectively. The higher stability of the OM(η^2-CS) isomer is not explored here, as no evidence for this product (or SM(η^2-CO)) was found in the spectra, as discussed later. Relative B3LYP energies and calculated structures for the SMCO and the OMCS insertion products are given in Figure 6.

Discussion

Group 4 metal atom reactions with CS_2 and OCS will be described separately, and the resulting S−M−CS, S−M(η^2-CS),

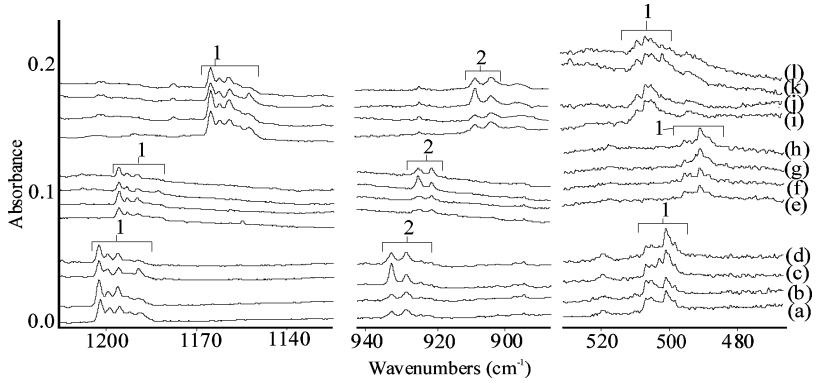

Figure 2. Infrared spectra in the 1210−1130, 940−890, and 530−460 cm^{-1} regions for Zr and CS_2. (a) After 30-min ablation of Zr with 0.5% $^{12}C^{32}S_2$ co-deposited in argon at 8 K, (b) after 10 min of mercury arc lamp irradiation $\lambda > 290$ nm, (c) after annealing to 25 K, and (d) after 10 min broad-band ($\lambda > 220$ nm) irradiation. (e) Deposition of Zr + $^{12}C^{34}S_2$, (f) $\lambda > 290$ nm irradiation, (g) annealing to 25 K, and (h) broad-band irradiation. (i) Deposition of Zr + $^{13}C^{32}S_2$, (j) $\lambda > 290$ nm irradiation, (k) annealing to 25 K, and (l) broad-band irradiation. Labels 1 and 2 refer to the SZrCS and SZr(η^2-CS) products, respectively.

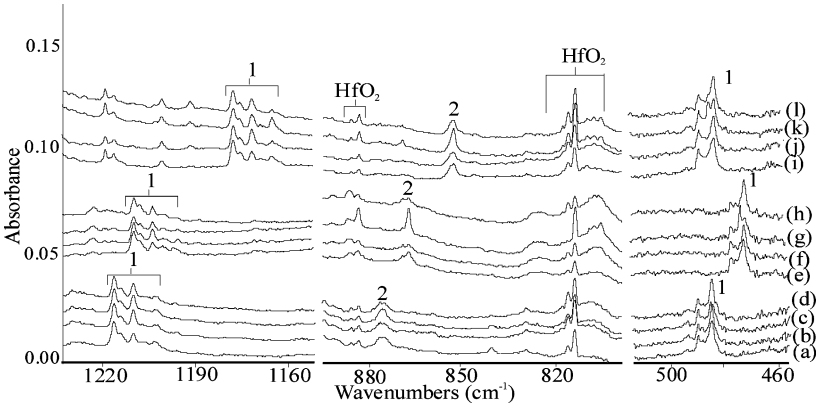

Figure 3. Infrared spectra in the 1230−1160, 890−810, and 520−460 cm^{-1} regions for Hf and CS_2. (a) After 30-min ablation of Hf with 0.5% $^{12}C^{32}S_2$ co-deposited in argon at 8 K, (b) after 10 min of mercury arc lamp irradiation $\lambda > 290$ nm, (c) after annealing to 25 K, and (d) after 10 min broad-band ($\lambda > 220$ nm) irradiation. (e) Deposition of Hf + $^{12}C^{34}S_2$, (f) $\lambda > 290$ nm irradiation, (g) annealing to 25 K, and (h) broad-band irradiation. (i) Deposition of Hf + $^{13}C^{32}S_2$, (j) $\lambda > 290$ nm irradiation, (k) annealing to 25 K, and (l) broad-band irradiation. Labels 1 and 2 refer to the SHfCS and SHf(η^2-CS) products, respectively.

TABLE 4: Observed Frequencies and Frequencies and Intensities Calculated at Different Levels of Theory for the S−M−C═O and O−M−C═S Products in the Group 4 Metal Atom and OCS Reactions[a]

(a) S−M−C═O

	S−Ti−C═O			S−Zr−C═O			S−Hf−C═O		
approx mode	obs	calc[b]	int	obs	calc[b]	int	obs	calc[b]	int
C═O stretch	1878.7/1858.5	1978.2	1038	1882.3/1868.3	1945.2	1119	1854.9/1844.5	1923.9	1058
M−S stretch	548.8	571.4	75	504.5	516.3	63		484.7	46
M−C stretch		484.9	3		437.6	2		456.2	7
O−C−M bend		362.6	3		354.6	50		433.8	3
O−C−M bend o.p.		337.1	31		345.2	2		356.1	2
S−M−C═O distort		98.4	5		92.3	3		93.3	2

(b) O−M−C═S

	O−Ti−C═S			O−Zr−C═S			O−Hf−C═S		
approx mode	obs	calc[b]	int	obs	calc[b]	int	obs	calc[b]	int
C═S stretch	1227.1	1248.6	261	1196.7	1222.1	339	1211.6	1234.1	261
M−O stretch	962.6	1029.5	347	883.4	921.0	225	880.3	889.9	180
M−C stretch		436.0	12		386.7	8		376.8	8
S−C−M bend		287.2	6.4		277.6	4		287.6	3
S−C−M bend o.p.		205.0	72.8		219.0	65		240.2	53
S−M−C═S distort		118.7	19.0		119.6	17		124.0	17

[a] Frequencies and intensities are in cm^{-1} and km/mol. Intensities are all calculated values. [b] B3LYP/6-311+G(2d)/SDD.

S−M−CO, O−M−CS, and M−(η^2-CO)S products will be identified from matrix IR spectra and DFT frequency calculations.

Ti + CS_2. Four new absorptions were observed at 1228.6, 1223.9, 1219.6, and 1212.9 cm^{-1} in the titanium experiments (labeled 1 in Figure 1). These peaks behaved as one product,

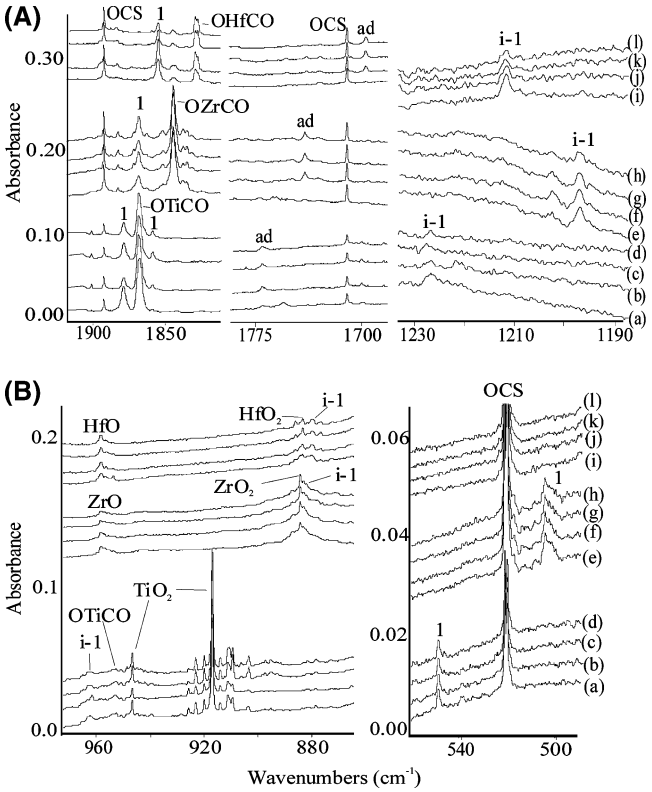

Figure 4. Infrared spectra in the 1910−1840, 1775−1700, 1230−1190, 970−950, and 550−500 cm^{-1} regions for group 4 metals and OCS. (a) After 30-min ablation of Ti co-deposited with 0.5% OCS at 8 K in an argon matrix, (b) after 10 min of mercury arc lamp irradiation $\lambda > 290$ nm, (c) after annealing to 25 K, and (d) after 10 min broad-band ($\lambda > 220$ nm) irradiation. (e) Deposition of Zr with 0.5% OCS, (f) $\lambda > 290$ nm irradiation of Zr + OCS, (g) after annealing to 25 K, and (h) after 10 min broad-band ($\lambda > 220$ nm) irradiation. (i) Deposition of Hf with 0.5% OCS, (j) $\lambda > 290$ nm irradiation of Hf + OCS, (k) after annealing to 25 K, and (l) after 10 min broad-band ($\lambda > 220$ nm) irradiation. Labels 1 and i-1 refer to the SMCO and OMCS products, respectively, and ad denotes the M(η^2-CO)S adduct. The weak OCS absorptions in the upper region are due to overtone and combination bands.

increasing 2-fold during visible ($\lambda > 470$ nm, not shown in Figure 1) and ultraviolet ($\lambda > 290$ nm) irradiation but decreasing on annealing. Furthermore, the bands shifted to approximately 1221.6, 1217.0, 1212.7, and 1208.1 cm^{-1} with $^{12}C^{34}S_2$ and to 1190.8, 1185.9, 1181.7, and 1175.8 cm^{-1} with $^{13}C^{32}S_2$. The isotopic 12−32/13−32 frequency ratio of 1.0316 and 12−32/12−34 frequency ratio of 1.0040 suggest a C═S stretching vibration. This is higher carbon character and lower sulfur character than that of the diatomic CS molecule (1.0291, 1.0081 ratios), the absorption of which has been observed at 1275.1 cm^{-1}.[15] The consistency between the isotopic ratios, combined with the almost identical photolysis and annealing behaviors, is evidence for multiple matrix sites of a single product, which has been previously shown elsewhere.[5] A second set of product absorptions (labeled 2) was also observed in this experiment at 963.0, 956.8, and 952.4 cm^{-1} with CS_2. Using $^{13}C^{32}S_2$, the same peaks shifted to 936.7, 931.1, and 926.9 cm^{-1} and to 954.9, 948.7, and 944.4 cm^{-1} with $^{12}C^{34}S_2$. These three absorptions had an isotopic 12−32/13−32 frequency ratio of 1.0275 and a 12−32/12−34 frequency ratio of 1.0084. Despite the lower carbon character and slightly higher sulfur character of this mode, the ratios are near those for diatomic CS and imply a C−S stretching vibration. The behavior of these three peaks was similar: they were weak on sample deposition, increased

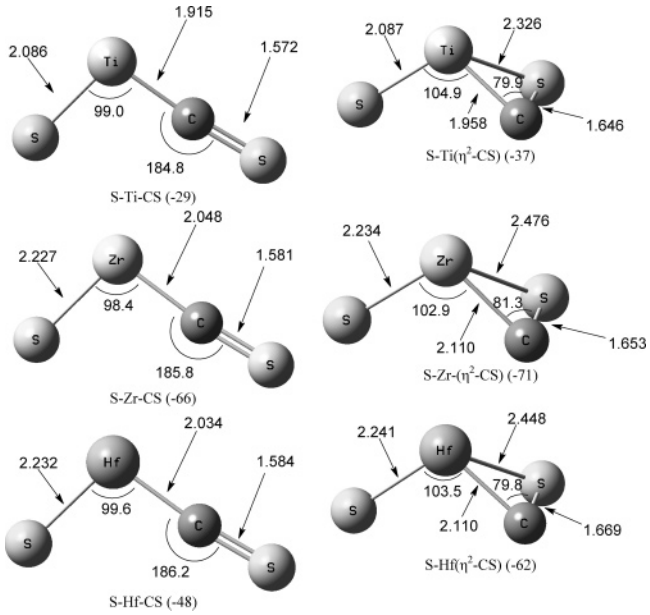

Figure 5. Calculated B3LYP structures (angstroms and degrees) and energies (kcal/mol) relative to M + CS_2 for the group 4 SMCS and SM(η^2-CS) products.

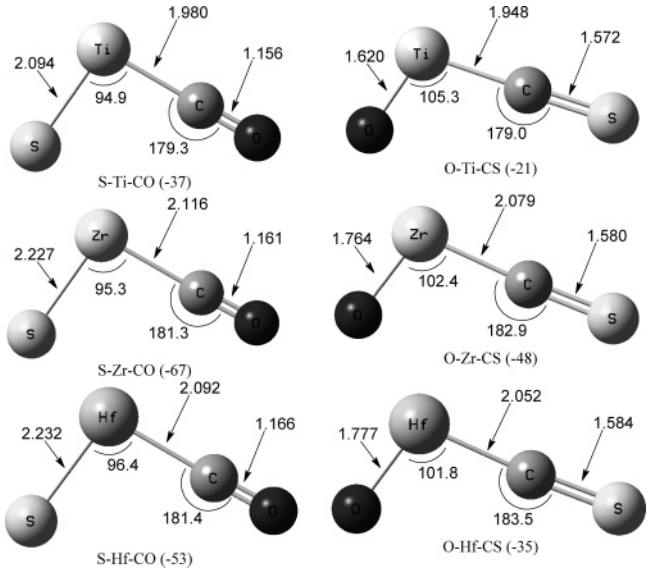

Figure 6. Calculated B3LYP structures (angstroms and degrees) and energies (kcal/mol) relative to M + OCS for the group 4 SMCO and OMCS products.

during visible and ultraviolet photolysis, and reached maximum intensity on annealing. Again, both isotopic ratios and behavior confirm that these are matrix sites of a single product.

In the lower region of the spectra, a new absorption was observed at 553.6 cm^{-1}. The band shifted to 553.5 cm^{-1} with $^{13}C^{32}S_2$ and to 543.5 cm^{-1} with $^{12}C^{34}S_2$. The ^{34}S isotopic shift is much larger that that of ^{13}C and indicates a high sulfur-character vibrational mode. Moreover, previous work has found Ti−S stretching modes to fall in this region.[19] This peak, although weak after ablation, increased substantially upon photolysis, almost mirroring the behavior of the upper frequency C═S stretching mode. Similar behavior was also observed for the isotopic counterparts.

Experimental and calculated vibrational frequencies, in conjunction with isotopic frequency ratios, were used to make two assignments. The lower C−S stretching peaks (963.0, 956.8, and 952.4 cm^{-1}) exhibited similar behavior and agreed well

with calculated C−S vibration for S−Ti(η^2-CS). The higher frequency C═S stretching modes (1228.6, 1223.9, 1219.6, and 1212.9 cm^{-1}) and the low Ti−S vibration (553.6 cm^{-1}) resembled the calculated frequencies of S−Ti−CS. This calculation also predicted a weak Ti−S stretch at a slightly higher frequency for S−Ti(η^2-CS), contrasting the large predicted intensity of the Ti−S stretch of S−Ti−CS, which supports assignment of the experimental band to the S−Ti−CS molecule. Values for both calculated and observed products are detailed in Table 1. Notice that the B3LYP frequencies are higher than the BPW91 calculated values: Most of the calculated frequencies are slightly higher than the observed values as expected.[18]

Zr + CS_2. Similar to results of Ti + CS_2, in experiments with Zr, product absorptions were observed at 1202.5, 1199.5, 1196.2, and 1189.4 cm^{-1} (labeled 1 in Figure 2) and increased slightly on sequential photolysis but decreased on subsequent annealing. These shifted to 1165.2, 1162.2, 1159.1, and 1152.4 cm^{-1} with $^{13}C^{32}S_2$ and to 1195.9, 1193.2, 1189.7, and 1182.9 cm^{-1} with $^{12}C^{34}S_2$. The four peaks had consistent isotopic frequency ratios, a 12−32/13−32 frequency ratio of 1.0321 and a 12−32/12−34 frequency ratio of 1.0055. These ratios are higher than those of diatomic CS and of the observed ratios with Ti, indicating that mode mixing is changing with the metal. Again, the four bands are matrix sites (matrix host−guest molecule trapping configurations) rather than different products. A second set of product bands appeared at 933.4 and 929.1 cm^{-1} (labeled 2) on deposition, increased on photolysis, and reached a maximum intensity on annealing. These shifted to 908.3 cm^{-1} with $^{13}C^{32}S_2$ and to 925.6 cm^{-1} with $^{12}C^{34}S_2$ and had the 12−32/13−32 ratio of 1.0282 and a 12−32/12−34 ratio of 1.0084. These bands were also attributed to matrix site splitting of a C−S stretch; the lower carbon and higher sulfur characters of the absorption compare favorably to lone CS. The two distinct behaviors of these bands, coupled with the previous Ti result, indicate two distinct products. The higher frequency C═S stretch is assigned to the S−Zr−CS molecule because of similarities between predicted and experimental vibrational frequencies, and the lower frequency mode is ascribed to the S−Zr(η^2-CS) molecule.

Previous work has found the Zr−S stretching frequency to fall around 500 cm^{-1}.[19] In our experiment, absorption was observed in this region at 502.5 cm^{-1}. The band was of moderate intensity and appeared to track with the upper C═S absorptions on irradiation and annealing. Furthermore, the calculated position and intensity favor assignment to the Zr−S stretch in S−Zr−CS (Table 2).

Hf + CS_2. The same matrix splitting found in Ti and Zr experiments was also observed for Hf with CS_2. Absorptions at 1216.4, 1214.3, 1210.0, and 1203.4 cm^{-1} shifted to 1177.8, 1175.6, 1171.7, and 1165.2 cm^{-1} with $^{13}C^{32}S_2$ and to 1210.0, 1207.9, 1203.9, and 1195.8 cm^{-1} with $^{12}C^{34}S_2$ (labeled 1 in Figure 3). These peaks are attributed to mostly C═S stretching because of a 12−32/13−32 frequency ratio of 1.0328 and a 12−32/12−34 ratio of 1.0064. However, an antisymmetric M−C−S character is developing, as indicated by the higher carbon and lower sulfur isotopic frequency ratios and character of this mode. The second C−S stretch was observed at 875.1 cm^{-1}, shifting to 852.9 cm^{-1} with $^{13}C^{32}S_2$ and to 867.6 cm^{-1} with $^{12}C^{34}S_2$ (labeled 2 in Figure 3). A 12−32/13−32 ratio of 1.0260 and a 12−32/12−34 ratio of 1.0086 were recorded. Again, the C−S stretching assignment was confirmed by isotopic ratios comparable to those of diatomic CS. The carbon character of this mode is lower than those observed with Ti and Zr, as discussed later. In the Hf−S stretching region,[19] the major absorption was observed at 484.9 cm^{-1}, which shifted to 473.1 cm^{-1} with $^{12}C^{34}S_2$ and to 484.9 cm^{-1} with $^{13}C^{32}S_2$. The intensity and behavior of this band appeared like that of the upper band system labeled 1. Accordingly, the higher frequency C═S stretch and the lower frequency Hf−S stretch are assigned to the S−Hf−CS molecule, as found in the Ti and Zr experiments. The lower frequency C−S stretch is attributed to S−Hf(η^2-CS).

Ti + OCS. Product bands were observed at 1878.7, 1866.8, 1858.5, 1769.2, 1227.1, 962.6, and 548.8 cm^{-1}. The peak at 1866.8 cm^{-1} decreased during long wavelength photolysis and increased during short wavelength photolysis and annealings. The band at 1878.7 cm^{-1} increased with short wavelength photolysis, decreased with long wavelength photolysis, and increased with annealing. Previous work has assigned the 1866.8 cm^{-1} band to O−Ti−CO.[4] The weak 1858.5 cm^{-1} band is probably a matrix site splitting as seen in the analogous CS_2 experiments. The peak at 1878.7 cm^{-1} is considered as a separate product because of distinct behavior. The band at 1769.2 cm^{-1} did not change noticeably with either photolysis or annealing. The weak product at 1227.1 cm^{-1} was observed to be of highest intensity on deposition, and further irradiation or annealing produced a decrease in signal, and the 962.6 cm^{-1} band behaved similarly.

Relative energy arguments narrow the range of possible products in OCS experiments. As mentioned above, STiCO was predicted to be more stable than OTiCS: the CO insertion product was computed to be 16−19 kcal/mol higher in energy than the CS insertion product for the group 4 metal atoms. Additionally, the product absorptions can be divided into regions on the basis of previous studies. Peaks between 1800 and 1900 cm^{-1} have previously been attributed to metal insertion product terminal CO stretching mode.[4] The peak at 1878.7 cm^{-1} falls neatly in this region and can be assigned to the STiCO product (labeled 1 in Figure 4). In experiments with Ti and CO_2, the CO stretch of the preinsertion adduct Ti(η^2-CO)O was observed at 1730 cm^{-1},[20] indicating that a band at 1769.2 cm^{-1} is reasonable for the CO stretch of the analogous Ti−(η^2-CO)S adduct (labeled ad in Figure 4). The presence of this simple adduct in the spectra could be further evidence of the higher energy required for CO insertion. With the CS_2 reagent, terminal CS stretching modes were found around 1200 cm^{-1}.[5] Therefore, the band at 1227.1 cm^{-1} is a C═S stretch, and it invites consideration of C−O insertion to form the OTiCS isomer product (labeled i-1 in Figure 4). Diatomic TiO has been found at 953 cm^{-1},[16] and TiS has been observed at 557.6 cm^{-1}.[19] By extension, the peaks at 962.6 and 548.8 cm^{-1} are most likely to be Ti═O and Ti═S stretching modes, respectively, of the isomeric OTiCS and STiCO products. Notice the relative absorbance of the 1878.7 and 1227.1 cm^{-1} bands (0.029 and 0.001): Scaling this by the calculated relative intensities (1038 and 261 km/mol from Table 4) predicts that the relative yield of the STiCO and OTiCS products in these experiments is 7 to 1, which is in line with the computed relative product stabilities (STiCO is 16 kcal/mol lower in energy than OTiCS).

Calculated frequencies with both B3LYP and BPW91 methods added more evidence for these assignments. The predicted CO stretching frequency of S−Ti−CO was 1978.2 cm^{-1} with B3LYP and 1881.5 cm^{-1} with BPW91. Therefore, the slightly lower frequency band at 1878.7 cm^{-1} is appropriate for this mode.[18] Furthermore, the Ti−S stretch of the same molecule was predicted at 571.4 cm^{-1} with B3LYP and 565.2 cm^{-1} with BPW91. These values are in good agreement with the experimental value of 548.8 cm^{-1}, showing further evidence for

S−Ti−CO as a product. The predicted frequencies of 1248.6 cm^{-1} with B3LYP and of 1217.4 cm^{-1} with BPW91 for O−Ti−CS show good agreement with the band at 1227.1 cm^{-1}. Moreover, the predicted oxide band of O−Ti−CS was 1029.5 cm^{-1} with B3LYP and 1001.3 cm^{-1} with BPW91, which correlated well with the 962.6 cm^{-1} absorption. No evidence was found for a Ti−(η^2-CS)O product, perhaps because of a lower energy barrier for CS insertion, which is supported by the weak 1769.2 cm^{-1} absorption for the Ti−(η^2-CO)S adduct.

Zr + OCS. Zirconium reactions with OCS produced bands at 1882.3, 1868.3, 1844.5, 1739.2, 1196.7, 883.4, and 504.5 cm^{-1}. The absorption at 1868.3 cm^{-1} increased during long wavelength photolysis and after annealing but decreased on photolysis at short wavelengths. Bands at 1739.2, 883.4, and 504.5 cm^{-1} did not change drastically with either photolysis or annealing. However, the very weak absorption at 1196.7 cm^{-1} was strongest after deposition; further photolysis and annealing caused a decrease in intensity.

Although no data has been published for reactions of Zr and CO_2, using similar logic as with Ti and OCS, one can separate the absorptions into groups on the basis of spectral region. The bands at 1882.3, 1868.3, and 1844.5 cm^{-1} all fall into the metal insertion product CO stretching region. The peak at 1739.2 cm^{-1} is appropriate for a CO stretch of the M−(η^2-CO)S preinsertion adduct. The band at 1196.7 cm^{-1} falls in the CS stretching region for the S−M−CS and O−M−CS molecules, while the 883.4 and 504.5 cm^{-1} peaks are in the Zr═O and Zr═S stretching regions, respectively.[16,19] Calculations confirm these assignments. The CO stretch of S−Zr−CO had a predicted frequency of 1945.3 cm^{-1} with B3LYP and 1859.2 cm^{-1} with BPW91. These are appropriate for the experimental frequency of 1868.3 cm^{-1}. Then, the peak at 1844.5 cm^{-1} is due to the CO stretch of the O−Zr−CO product from the CO_2 impurity. The major band at 1844.5 cm^{-1} differs from the 1868.3 cm^{-1} CO stretch of S−Zr−CO by almost the same amount as the titanium analogues. Additionally, the predicted Zr−S stretch of S−Zr−CO (516.3 cm^{-1} with B3LYP and 510.2 cm^{-1} with BPW91) agrees well with the experimental frequency in this region (504.5 cm^{-1}). This is additional evidence for the presence of the S−Zr−CO product. The weak absorption at 1196.7 cm^{-1} agreed well with the CS stretch of O−Zr−CS (predicted frequencies of 1222.2 with B3LYP and 1196.3 with BPW91). Moreover, 883.4 cm^{-1} is similar to the oxide band of the same molecule, which had a predicted frequency of 921.0 cm^{-1} with B3LYP and 896.8 cm^{-1} with BPW91. The band at 1739.2 cm^{-1} shows the necessary metal-dependent shift (with reference to the Ti experiment) to assign to the Zr−(η^2-CO)S adduct.

Hf + OCS. Observations with hafnium were very similar to those with titanium and zirconium. Product absorptions were observed at 1854.9, 1844.5, 1828.3, 1697.1, 1211.6, and 880.3 cm^{-1}. The band at 1854.9 cm^{-1} increased during short wavelength photolysis and annealing, decreasing only after photolysis at a long wavelength. The band at 1828.3 cm^{-1} increased when photolyzed at long wavelength and on annealing. However, the weak bands at 1211.6 and 880.3 cm^{-1} decreased on photolysis and annealing. Each of these peaks fell into regions, following those of titanium and zirconium. The band at 1854.9 cm^{-1} correlated with the predicted CO stretching frequency of S−Hf−CO (1923.9 cm^{-1} with B3LYP and 1846.3 cm^{-1} with BPW91). The predicted Hf−S stretching frequency for this molecule was 484.7 and 479.5 cm^{-1} with B3LYP and BPW91, respectively. This explains why no peak was observed experimentally, as it would fall in the noise at the lower limits of the spectra. The band at 1211.6 cm^{-1} is appropriate for the CS stretch of O−Hf−CS (calculated as 1234.1 and 1209.5 cm^{-1} with B3LYP and BPW91, respectively). The peak at 880.3 cm^{-1} agrees well with the hafnium oxide mode of the same molecule, which had a predicted frequency of 889.9 and 864.7 cm^{-1} using B3LYP and BPW91, respectively. Notice again that the major SHfCO band is stronger than the major OHfCS absorption, as a higher yield is expected for the more stable molecule, which supports the assignment of these molecules. The 1828.3 cm^{-1} band follows for OHfCO from CO_2 impurity. Finally, the absorption at 1697.1 cm^{-1} shows a similar metal-dependent shift as the Zr product in the same region and can therefore be assigned to the analogous Hf−(η^2-CO)S adduct.

Structural Isomerization. Reactions with group 4 metals and CS_2 produced two product types: an insertion product (S−M−CS) and a S−M(η^2-CS) cyclic isomer. Both are increased on sequential visible and ultraviolet photolysis, but annealing clearly favors the cyclic isomer at the expense of the insertion product, which suggests isomerization to the more stable cyclic isomer on annealing. This effect is more dramatic for Ti and Zr than for Hf, and it could arise from relaxation of new M + CS_2 products formed on annealing. This simple rearrangement is further supported by the absence of additional product molecules. With group 4 metals, the more stable adduct S−M(η^2-CS) was weak on sample deposition possibly owing to its photosensitivity to the laser-ablation plume. Furthermore, irradiation increased the intensity of the S−M−CS peaks (more so for the Ti than for the Hf species), while annealing produced a small decrease in intensity. As the relative energies of S−M−CS products are about 10 kcal/mol higher than the S−M(η^2-CS) form, structural isomerization during the annealing process is reasonable. Upon annealing, the matrix cage softens and the molecule returns to its most stable structural isomer, increasing the intensity of the S−M(η^2-CS) complex peaks. This process is outlined below

$$\text{S−M−CS} \xrightarrow[\text{annealing 25 K}]{} \text{S−M}(\eta^2\text{-CS})$$

Previous work found a reversible photochemical isomerization for the Sc + CO_2 reaction products, O−Sc−CO and O−Sc−(η^2-CO).[21] Later work on Ti and V reported photochemical rearrangement from OTiCO to O−Ti(η^2-CO) and from OVCO to OV(η^2-CO) products.[4] The relative stabilities of these cases were the opposite of results discussed in this work as the OMCO product was more stable than the OM(η^2-CO) adduct. For example, O−Sc−CO was computed to be more stable than O−Sc(η^2-CO) by about 5 kcal/mol.[21] The reversal of stabilities between open and ring structures and between groups 3 and 4 metal atoms is discussed in the comparison section below.

Group Trends. Group 4 trends in both experiments with CS_2 and OCS were almost as expected. Vibrational frequencies decreased going down the group for all modes of all molecules. The vibrational mechanics in this series was defined by examining the isotopic frequency ratios. As metal mass increased, the carbon character of the C═S stretch increased, increasing mode mixing and developing a more antisymmetric M−C−S motion, which further corroborates the SMCS structure and assignments. Geometries calculated for product molecules also revealed several trends. The S−Zr−C bond angles were smaller than those of S−Ti−C, but the S−Hf−C angle was larger than the S−Zr−C angle in all CS insertion products (SMCS, S−M(η^2-CS), and SMCO). The M−C−S angle did not change appreciably between the different SMCS adducts. The effect of relativistic contraction[22] was observed in several cases. In the SMCS, OMCS, and SMCO products, the M−C

bond length is shorter for Hf than for Zr. This accounts for a change in Hf−C, C═S coupling, and the observed and calculated C═S stretching frequency increase from OZr−C═S to OHf−C═S (Table 4). In the S−M(η^2-CS) complex with Zr and Hf, the M−C bond length remained constant, while the M−S bond length decreased for Hf. This relativistic contraction rationalizes the lower carbon and slightly higher sulfur character of the associated C−S mode in the ring complexes. Relativistic effects such as these are common with group 4 transition metals and have been observed with both metal oxides and hydrides.[16,23] In all products, the CS and CO bond lengths increased slightly with metal atomic mass in the complex.

Comparison to the CO_2 System and Previous CS_2 Systems. The previous study of CS_2 with Co, Ni, and Cu resulted in the products SMCS, M-CS_2, and M−(η^2-CS)S, while the S−M(η^2-CS) isomer was not observed.[5] Additionally, the SMCS product was determined to be the most stable. This directly contrasts reactions of group 4 metals and CS_2, where the S−M(η^2-CS) product isomer was found to be more stable. There are two explanations for this difference. The higher electron deficiency of the group 4 metals with respect to Co, Ni, and Cu explains the stabilization by withdrawing electron density from the CS bond. Moreover, the four valence electrons on the metal are ideal for η^2-bonding, and the S−M(η^2-CS) structure is more stable than the simple insertion product SMCS. This also explains the different relative stabilities of the previous group 3 OMCO and O−M(η^2-CO) complexes.[21] The more electron-deficient Sc, Y, and La atoms do not have enough valence electrons for both a metal oxide bond and a stable η^2 bridge bond. Therefore, the insertion species OMCO remains the most stable. Furthermore, we find that the relative yield of the side-bound S−M(η^2-CS) product as compared to SMCS is higher for SCS than for the OCO analogues.[4] This is in agreement with findings for transition-metal systems in synthetic chemistry.[17]

Our recent study of group 3 metal reactions with CS_2 and OCS supports these findings.[3] The SMCS product was found to be lower in energy, as in the Co, Ni, and Cu study. However, in the group 3 case, the S−M(η^2-CS) complex was observed to increase on ultraviolet photolysis. The difference in energy between the SMCS and S−M(η^2-CS) complexes was small enough to allow structural isomerization, in the opposite direction from that observed with group 4 metal species. This finding supports a valence shell dependence on the relative stabilities of these two product molecules. To maintain the lowest multiplicity, group 3 metal atoms prefer a doublet state SMCS structure, despite their electron deficiency. Because of their extra valence electron, group 4 metals favor a singlet S−M(η^2-CS) complex, which satisfies electron deficiency through bridge-bonding.

Another comparison can be made between the group 3 and 4 SMCS and SMCO insertion products. The terminal C═S and C═O stretching modes are 51 and 16 cm^{-1} lower, respectively, for the Ti than the Sc compounds, and 33 and 16 cm^{-1} lower for the Zr than the Y complexes. This chemical effect can be explained by electron density on the metal atom. The larger electron density of group 4 metal atoms results in more back-bonding into the antibonding orbitals of the C═O and C═S subunits, weakening the bonds and causing a decrease in frequency.

Conclusions

Laser-ablated titanium, zirconium, and hafnium atoms were reacted with CS_2 and OCS during condensation in an argon matrix. The SMCS and S−M(η^2-CS) product structural isomers were formed on sample deposition and increased by photolysis, but annealing favored the more stable cyclic isomer on the basis of DFT calculated energies. In contrast, the side-bound isomer is computed to be less stable for group 3 metals, and this isomer is absent from Co, Ni, and Cu reaction products. Group 4 metal reactions with OCS resulted in SMCO, OMCS, and M(η^2-CO)S products. The relatively higher energy of the CO insertion product with respect to the CS insertion product was manifested in lower product yields for the former. Product identifications were verified by isotopic substitution and by density functional vibrational frequency calculations.

Acknowledgment. Acknowledgment is made to the Donors of the American Chemical Society Petroleum Research Fund for support of this research.

References and Notes

(1) Cotton, F. A.; Wilkinson, G.; Murillo, C. A.; Bochmann, M. *Advanced Inorganic Chemistry*, 6th ed.; Wiley: New York, 1999.
(2) Fomitchev, D. V.; Bagley, K. A.; Coppens, P. *J. Am. Chem. Soc.* **2000**, *122*, 532.
(3) Baker, A. B.; Andrews, L. *J. Phys. Chem. A* **2006**, *110*, 10419 (group 3, SCS).
(4) Zhou, M.; Andrews, L. *J. Phys. Chem. A* **1999**, *103*, 2066.
(5) Zhou, M. F.; Andrews, L. *J. Phys. Chem. A* **2000**, *104*, 4394.
(6) Becke, A. D. *J. Chem. Phys.* **1993**, *98*, 5648.
(7) Lee, C. T.; Yang, W. T.; Parr, R. G. *Phys. Rev. B* **1988**, *37*, 785.
(8) Becke, A. D. *Phys. Rev. A* **1988**, *38*, 3098.
(9) Perdew, J. P.; Wang, Y. *Phys. Rev. B* **1992**, *45*, 13244.
(10) Frisch, M. J.; Trucks, G. W.; Schlegel, H. B.; Scuseria, G. E.; Robb, M. A.; Cheeseman, J. R.; Zakrzewski, V. G.; Montgomery, J. A.; Stratmann, R. E.; Burant, J. C.; Dapprich, S.; Millam, J. M.; Daniels, A. D.; Kudin, K. N.; Strain, M. C.; Farkas, O.; Tomasi, J.; Barone, V.; Cossi, M.; Cammi, R.; Mennucci, B.; Pomelli, C.; Adamo, C.; Clifford, S.; Ochterski, J.; Petersson, G. A.; Ayala, P. Y.; Cui, Q.; Morokuma, K.; Rega, N.; Salvador, P.; Dannenberg, J. J.; Malick, D. K.; Rabuck, A. D.; Raghavachari, K.; Foresman, J. B.; Cioslowski, J.; Ortiz, J. V.; Baboul, A. G.; Stefanov, B. B.; Liu, G.; Liashenko, A.; Piskorz, P.; Komaromi, I.; Gomperts, R.; Martin, R. L.; Fox, D. J.; Keith, T.; Al-Laham, M. A.; Peng, C. Y.; Nanayakkara, A.; Challacombe, M.; Gill, P. M. W.; Johnson, B.; Chen, W.; Wong, M. W.; Andres, J. L.; Gonzalez, C.; Head-Gordon, M.; Replogle, E. S.; Pople, J. A. *Gaussian 98*, Revision A.11.4; Gaussian, Inc.: Pittsburgh, PA, 2002.
(11) Krishnan, F.; Binkley, J. S.; Seeger, R.; Pople, J. A. *J. Chem. Phys.* **1980**, *72*, 650.
(12) Frisch, M. J.; Pople, J. A.; Binkley, J. S. *J. Chem. Phys.* **1984**, *80*, 3265.
(13) Andrae, D.; Haussermann, U.; Dolg, M.; Stoll, H.; Preuss, H. *Theor. Chim. Acta* **1990**, *77*, 123.
(14) (a) Bauschlicher, C. W., Jr.; Ricca, A.; Partridge, H.; Langhoff, S. R. In *Recent Advances in Density Functional Theory*, Part II.; Chong. D. P, Ed.; World Scientific Publishing: Singapore, 1997. (b) Zhou, M.; Andrews, L.; Bauschlicher, C. W., Jr. *Chem. Rev.* **2001**, *101*, 1931. (c) Zhao, Y.; Truhlar, D. G. *J. Chem. Phys.* **2006**, *124*, 224105.
(15) Zhou, M.; Andrews, L. *J. Chem. Phys.* **2000**, *112*, 6576.
(16) Chertihin, G. V.; Andrews, L. *J. Phys. Chem.* **1995**, *99*, 6356.
(17) Pandey, K. K. *Coord. Chem. Rev.* **1995**, *140*, 37.
(18) (a) Scott, A. P.; Radom, L. *J. Phys. Chem.* **1996**, *100*, 16502. (b) Bytheway, I.; Wong, M. W. *Chem. Phys. Lett.* **1998**, *282*, 219. (c) Andersson, M. P.; Uvdal, P. *J. Phys. Chem. A* **2005**, *109*, 2937.
(19) Liang, B. Y.; Andrews, L. *J. Phys. Chem. A* **2002**, *106*, 6295.
(20) Mascetti, J.; Tranquille, M. *J. Phys. Chem.* **1988**, *92*, 2177.
(21) Zhou, M.; Andrews, L. *J. Am. Chem. Soc.* **1998**, *120*, 13230.
(22) Pyykko, P. *Chem. Rev.* **1988**, *88*, 563.
(23) Chertihin, G. V.; Andrews, L. *J. Phys. Chem.* **1995**, *99*, 15004.